$ZnCo_2O_4$纳米颗粒组装的毛线团状的微球用于锂离子电池负极材料

王 瑛*,[1] 林 宁[2]
([1]山东玉皇新能源技术有限公司,菏泽 274000)
([2]中国科学技术大学化学与材料科学学院,合肥 230026)

摘要:通过液相共沉淀法获得Zn和Co的前驱,经过600 ℃煅烧处理获得$ZnCo_2O_4$纳米颗粒组装的毛线团状的微球。电化学测试表明,在0.5 $A\cdot g^{-1}$的电流密度下循环200次可逆比容量保持为965 $mAh\cdot g^{-1}$;在0.8 $A\cdot g^{-1}$的电流密度下循环350次可逆比容量保持为882 $mAh\cdot g^{-1}$。倍率性能测试表明在2 $A\cdot g^{-1}$的电流密度时可逆比容量为736 $mAh\cdot g^{-1}$。

关键词:$ZnCo_2O_4$;纳米颗粒;线团状微球;锂离子电池
中图分类号:TM912 **文献标识码**:A **文章编号**:1001-4861(2016)12-2191-07
DOI:10.11862/CJIC.2016.259

Clew-like Microspheres Composed of Uniform $ZnCo_2O_4$ Nanoparticles as Anode Material for Lithium-Ion Batteries

WANG Ying*,[1] LIN Ning[2]
([1]*Shandong Yuhuang New Energy Technology Co., Ltd., Heze, Shandong* 274000, *China*)
([2]*Department of chemistry, University of Science and Technology of China, Hefei* 230026, *China*)

Abstract: Clew-like microshperes, composed of $ZnCo_2O_4$ nanoparticles, are synthesized by heat treatment of co-precipitated Zn and Co contained precursor at 600 ℃. As anode for Li ion battery, the obtained $ZnCo_2O_4$ microspheres deliver a reversible capacity of 965 $mAh\cdot g^{-1}$ at 0.5 $A\cdot g^{-1}$ after 200 cycles, and the capacity of the $ZnCo_2O_4$ microspheres still remains 882 $mAh\cdot g^{-1}$ at 0.8 $A\cdot g^{-1}$ over 350 cycles. The rate capability shows that a reversible capacity of 736 $mAh\cdot g^{-1}$ is maintained at high current density of 2.0 $A\cdot g^{-1}$.

Keywords: $ZnCo_2O_4$; nanoparticles; clew-like microspheres; lithium-ion batteries

0 Introduction

Recently, spinel type $ZnCo_2O_4$ has been considered as an attractive anode material because both Zn and Co are electrochemical active for lithium storage [1-2], thus resulting in higher theoretical capacity (975 $mAh\cdot g^{-1}$) than pure Co_3O_4 (890 $mAh\cdot g^{-1}$)[3-6]. To improve the Li-ion storage performance, several efforts have been made to fabricate nanostructured $ZnCo_2O_4$ materials. Sharma et al. prepared porous $ZnCo_2O_4$ nanotubes which showed a reversible capacity of 900 $mAh\cdot g^{-1}$ at 60 $mA\cdot g^{-1}$ over 60 cycles[3]. The $ZnCo_2O_4$ nanorods prepared by hydrothermal method at 180 ℃ delivered a reversible capacity of 767 $mAh\cdot g^{-1}$ at 0.2 $mA\cdot cm^{-2}$ over 60 cycles[5]. Qiu et al. fabricated porous $ZnCo_2O_4$ nanoflakes which exhibited a capacity of 750

收稿日期:2016-06-22。收修改稿日期:2016-09-28。
*通信联系人。E-mail:yhwangying@163.com

mAh·g^{-1} at 80 mA·g^{-1} over 50 cycles[7]. Du et al. synthesized $ZnCo_2O_4$ nanowires via sacrificial templates, delivering a reversible capacity of 957 mAh·g^{-1} at 100 mA·g^{-1} over 20 cycles[8].

Mesoporous micro/nano-structures as an important family of functional materials have attracted considerable attention in recent years. This unique structure could take advantage of both micro and nano components, such as better permeability, large surface area, high tap density, and mechanical integrity[2-3,11]. Bai et al. prepared $ZnCo_2O_4$ 3D hierarchical twin microspheres that delivers a specific capacity of 550 mAh·g^{-1} at 5 A·g^{-1} for 2 000 cycles[12]. Wang et al. prepared mesoporous $ZnCo_2O_4$ microspheres which exhibited initial specific capacity of 1 332 mAh·g^{-1} at a current density of 100 mA·g^{-1}, and maintained at 721 mAh·g^{-1} after 80 discharge/charge cycles[13].

Herein, the hierarchical clew-like $ZnCo_2O_4$ microspheres composed of uniform nanoparticles were synthesized by a two-step method. First, a typical co-precipitation reaction is carried out to fabricate the sub-carbonate precursor. In this process, the Zn^{2+} and Co^{2+} are co-precipitated by bicarbonate ion to form a large amount of nanoparticles which would subsequently assemble as microspheres. Second, post-annealing treatment at 600 ℃ is able to decompose and oxidize the precursor. As an anode material for rechargeable lithium-ion batteries, the as-prepared $ZnCo_2O_4$ microspheres exhibit the reversible capacity of 965 mAh·g^{-1} at 500 mA·g^{-1} after 200 cycles, 882 mAh·g^{-1} at 800 mA·g^{-1} after 350 cycles, and good rate-capability with a capacity of 736 mAh·g^{-1} at 2.0 A·g^{-1}.

1 Experimental

1.1 Preparation of clew-like microspheres of $ZnCo_2O_4$

All of chemical reagents were of analytical grade and were used without any further purification. In a typical experiment, $ZnCo_2O_4$ microspheres were synthesized through two steps. Firstly, 0.294 5 g of $Zn(NO_3)_2$·$6H_20$, 0.584 97 g of $Co(NO_3)_2$·$6H_20$, and 3.964 g of $(NH_4)_2SO_4$ were dissolved in 210 mL deionized water, marked as solution A. 2.372 g of NH_4HCO_3 was dissolved in 210 mL deionized water, marked as solution B. 0.2 g of tartaric acid was dissolved in 21 mL absolute ethanol, marked as solution C. Then, the solution B and C were injected into solution A. After stirring vigorously at room temperature for 30 minutes, the mixed solution was sealed in glass beaker, which was heated at 60 ℃ for 9 hours. Subsequently, the pink precipitate was collected by centrifugation, washed by deionized water and absolute ethanol several times, and followed by vacuum-drying at 60 ℃ overnight.

Secondly, the as-prepared pink precursor was annealed at 600 ℃ in muffle furnace for 2 hours with a ramp rate of 2 ℃·min^{-1} under air atmosphere. Contrast experiment was carried out following the similar procedure without adding tartaric acid.

1.2 Characterization

The final product in this work was characterized by X-ray diffraction (XRD) on Philips X′Pert Super diffractometer with Cu $K\alpha$ radiation (λ=0.154 178 nm), the working voltage and current is 40 kV and 40 mA, respectively. The thermal performance of as-prepared precursor Zn-Co co-precipitation was studied by thermogravimetric analysis (TGA) on Micrometrics ASAO 2020M at a heating rate of 10 ℃·min^{-1} in air. The scanning electron microscope (SEM) images were taken by using a JEOL-JSM-6700F field-emitting (FE) scanning electron microscope with an accelerating voltage of 5 kV. The high-resolution transmission electron microscope (HRTEM) was taken on a JEOL-2010 transmission electron microscope at an accelerating voltage of 200 kV. Brunauer-Emmett-Teller (BET) surface area and Barrett-Joyne-Halenda (BJH) pore distribution plots were calculated on basis of the N_2 absorption-desorption isotherms that were measured on Micromeritics ASAP 2020 accelerated surface area and porosimetry system. Surface analysis by X-ray photoelectron spectra (XPS) was performed on VGESCA-LABMKIIX-ray photoelectronic spectrometer.

1.3 Electrochemical measurements

Half-cell tests were conducted using two electrode coin cells (CR2016) with pure Li metal foil as counter electrode. For preparing working electrode, a slurry mixture of as-prepared active material, super

P, and PVDF at a weight ratio of 80:10:10, was coated on copper foil (99.9%). The active material density of each electrode was determined to be about 1.5 mg·cm^{-2}. A solution of 1 mol·L^{-1} $LiPF_6$ in ethylene carbonate (EC) and diethyl carbonate (DEC) (1:1, V/V) was served as electrolyte. The cells were assembled in an argon-filled glove box. Galvanostatic charge/discharge measurements were carried out on a LAMD-CT2001A instrument with a fixed voltage range of 0.005~3.0 V (vs Li^+/Li). Cyclic voltammetry (CV) was performed on electrochemistry workstation (CHI 660D), with a scanning rate of 0.1 mV·s^{-1} at room temperature. Electrochemical impedance spectroscopy (EIS) was measured with an electrochemical station (CHI 660D) by applying an AC voltage of 5 mV in the frequency ranging from 100 kHz to 0.04 Hz.

2 Results and discussion

Fig.1a shows the thermogravimetric analysis (TGA) curves of the co-precipitated precursor. The first weight loss of 27.69% before 183 ℃ mainly corresponds to the evaporation of absorbed moisture and the loss of lattice water of the precipitation. As the temperature further increases, the 26.9% weight loss between 183 and 325 ℃ is assigned to the complete decomposition of co-precipitated metal (cobalt and zinc) carbonates. At 600 ℃, there is no significant weight change, and high temperature treatment would improve the crystallinity of the product.

The crystalline structure and phase information of the product were verified by powder X-ray diffraction (XRD) patterns, as shown in Fig.1b. Eight main peaks at 18.97°, 31.22°, 36.79°, 38.49°, 44.74°, 55.57°, 59.36° and 61.36° are attributed to the diffraction peaks of (111), (220), (311), (222), (400), (422), (511), (440) and (533) planes of cubic spinel $ZnCo_2O_4$ (a=0.809 64 nm, space group $Fd\bar{3}m$, PDF card No.23-1390). The Zn^{2+} and Co^{3+} ions occupy the tetrahedral sites and the octahedral sites in this crystal structure, respectively. Based on the full width at half maximum (FWHM) of the main diffraction peaks, the primary particle size of obtained sample was calculated to be about 32 nm using Scherrer′s equation: $D=K\lambda/(B\cos\theta)$, where K is Scherrer constant, B is FWHM, λ is radiation wavelength, θ is diffraction angle.

The surface electronic state and the composition of the obtained $ZnCo_2O_4$ were analyzed by X-ray photoelectron spectra (XPS). The binding energies for the C1s peak (284.6 eV) are served as correction in the XPS analysis. Fig.2a exhibited a typical XPS spectrum which is consisted of Zn, Co, O, and C elements. No other impure peaks were observed. Fig. 2b presented the high-resolution Zn2p spectrum, in which two strong peak at 1 020.5 and 1 043.9 eV were ascribed to Zn2$p_{1/2}$ and Zn2$p_{3/2}$ orbits of Zn(Ⅱ), respectively. Fig.2c showed the deconvoluted Co2p spectrum, where two main peaks are centered at 794.9 eV for Co2$p_{3/2}$ and 780 eV for 2$p_{1/2}$, indicating the Co(Ⅲ) oxidation state formed in this composition. Fig.2d displays the major O1s peak located at 529.95 and 531.5 eV, which suggests the oxygen species of the Co-O and Zn-O in $ZnCo_2O_4$.

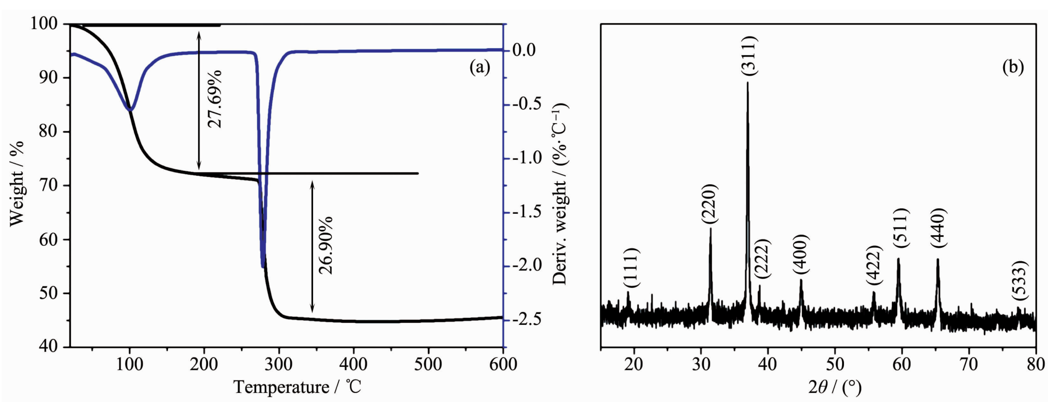

Fig.1 (a) Thermogravimetric analysis (TGA) and deriv. weight curves of the precursor heated in air; (b) XRD pattern of the as-synthesized $ZnCo_2O_4$

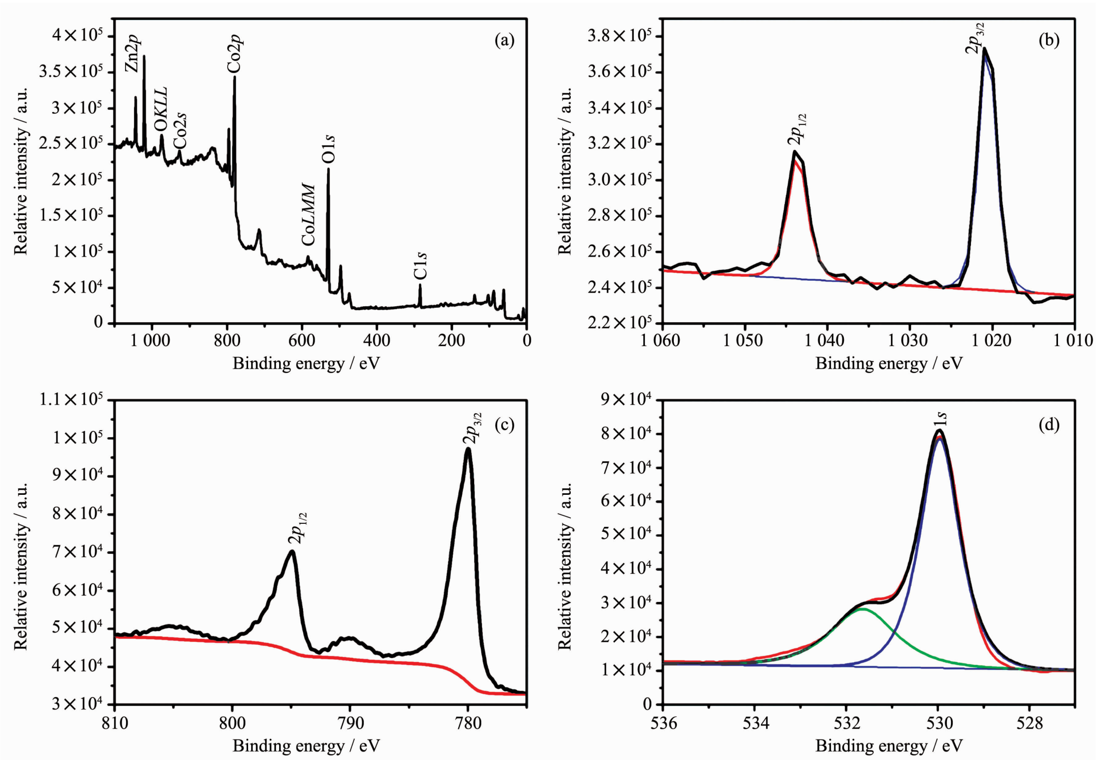

Fig.2 XPS spectra: survey spectrum (a), Zn2*p* (b), Co2*p* (c) and O1*s* (d) for $ZnCo_2O_4$ sample

The structure and morphology of the synthesized $ZnCo_2O_4$ was investigated by scanning electron microscope (SEM) and transmission electron microscope (TEM) images. As shown in Fig.3a, the obtained sample exhibits clew-like microspheres with an average diameter of 2~3 μm. Fig.3b shows the higher magnification image of the chapped microspheres. It was clearly observed that those hierarchical microspheres are composed of interconnected uniform nanoparticles with a mean size of ~30 nm. Obviously, these nanoparticles would allow for better release of stress without the mechanical fracture during cycling[3]. Fig.S1 shows the sample prepared from contrast experiment without using tartaric acid, which is consisted of disordered nanoparticles. So, it was reasonable to believe that the tartaric acid played an important role in constructing the clew-like $ZnCo_2O_4$ microspheres. Fig.3d showed the HRTEM image. The measured d-spacing of lattice fringe was 0.461 nm, corresponding to the (111) plane of cubic spinel $ZnCo_2O_4$ crystals.

Fig.3c shows the N_2 adsorption-desorption isotherms at 77 K, and the corresponding pore size distribution calculated by Barrett-Joyne-Halenda (BJH) method from the desorption branch. The BET specific surface area of the $ZnCo_2O_4$ microspheres is 8 $m^2 \cdot g^{-1}$, associated with a pore volume of 0.055 $cm^3 \cdot g^{-1}$. The pore size is ranging from 10 to 110 nm, with an average size of 46.7 nm. The porous hierarchical structure could provide a channel for electrolyte to contact with active materials completely, making sure of the effective lithium ion/electron diffusion between the solid/liquid interfaces.

The electrochemical properties of the as-synthesized $ZnCo_2O_4$ microspheres were first investigated by cyclic voltammogram (CV), as shown in Fig.4. In the first cycle, the sharp cathodic peak at 0.86 V is assigned to the reduction of $ZnCo_2O_4$ by Li to Zn^0 and Co^0[3]. Two broad oxidation peaks located at 1.8 V and 2.2 V in the first anodic scan are attributed to the oxidation of Zn to Zn^{2+} and Co to Co^{3+}, respectively. In the subsequent cycles, the reduction peaks are gradually shifted to 1.0 V and became much broader, which implies the irreversible electrochemical reaction during the first discharge process[13,15]. From second cycle forward, the CV curves are overlapped very

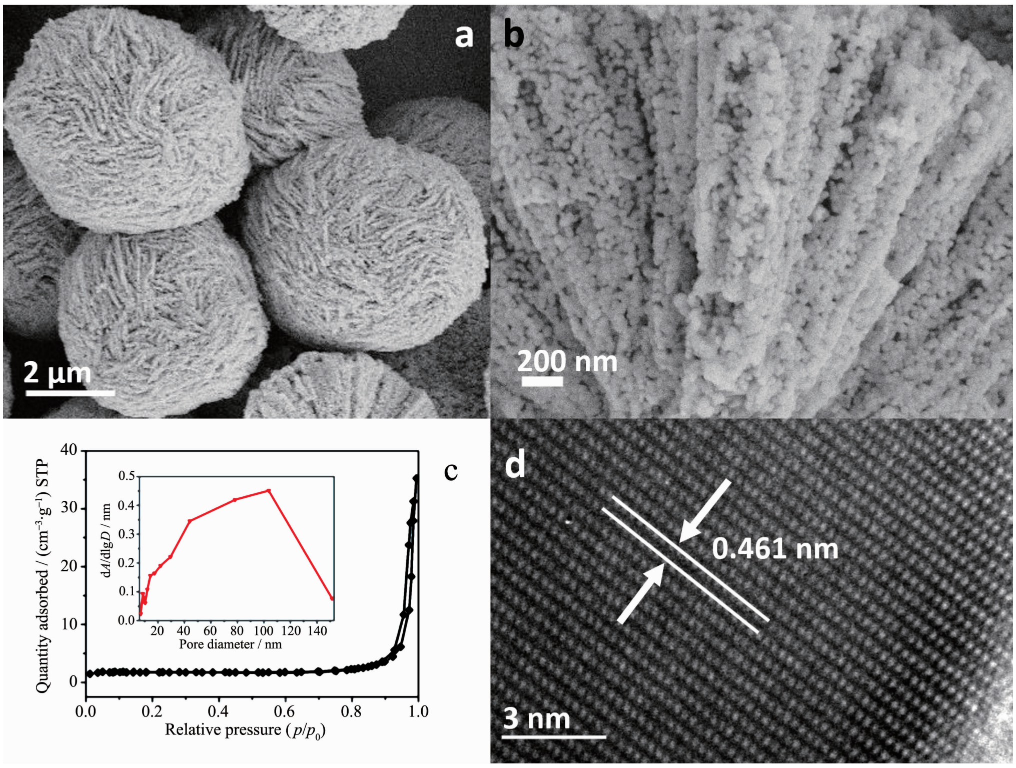

Fig.3　(a) SEM image of the obtained $ZnCo_2O_4$ microspheres; (b) SEM image of the chapped surface of $ZnCo_2O_4$ microspheres; (c) Typical nitrogen adsorption isotherms and corresponding BJH pore size distribution; (d) HRTEM image of the as-synthesized $ZnCo_2O_4$ sample

well, indicating the good reversible electrochemical reactions. Base on the above analysis, the lithium-ion insertion/extraction reaction with $ZnCo_2O_4$ microspheres could be determined as the following equations **1~5**[3]:

$$ZnCo_2O_4+8Li^++8e^- \longrightarrow Zn+2Co+4Li_2O \quad (1)$$

$$Zn+Li^++e^- \longrightarrow LiZn \quad (2)$$

$$Zn+Li_2O \longrightarrow ZnO+2Li^++2e^- \quad (3)$$

$$Co+Li_2O \longrightarrow CoO+2Li^++2e^- \quad (4)$$

$$3CoO+Li_2O \longrightarrow Co_3O_4+2Li^++2e^- \quad (5)$$

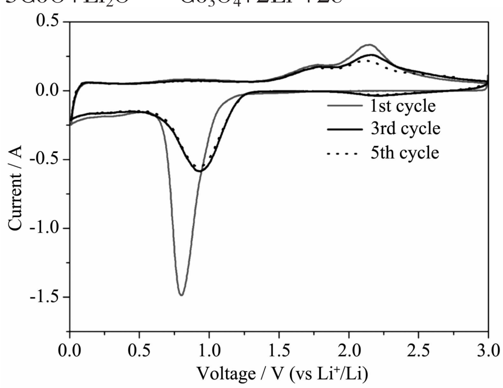

Fig.4　Cyclic voltammograms (1st, 3rd and 5th cycles) of $ZnCo_2O_4$ microspheres electrode

Fig.5a shows the discharge and charge profiles of $ZnCo_2O_4$ microspheres at a current density of 0.2 $A\cdot g^{-1}$. In the first discharge curve, there was a clear potential plateau located at near 1 V (vs Li^+/Li), and the overall specific capacity was as high as 1 260 $mAh\cdot g^{-1}$, the initial charge capacity is 832 $mAh\cdot g^{-1}$. The large irreversible capacity is caused by the irreversible equation **1** and the formation of unstable solid electrolyte interphase (SEI). From the second cycle onward, the long potential plateau was replaced by a sloping discharge curves, which is similar to previous reports[13-14]. Noteworthy, the charge/discharge curves are overlapped well for the second and third cycles.

Fig.5b exhibits the cycling behavior of the $ZnCo_2O_4$ microspheres at a current density of 0.5 $A\cdot g^{-1}$ and the corresponding coulombic efficiency. At a current density of 0.5 $A\cdot g^{-1}$, the electrode delivers a reversible capacity of 965 $mAh\cdot g^{-1}$ over 200 cycles, which was further higher than that of graphite (372 $mAh\cdot g^{-1}$). The coulombic efficiency increases from

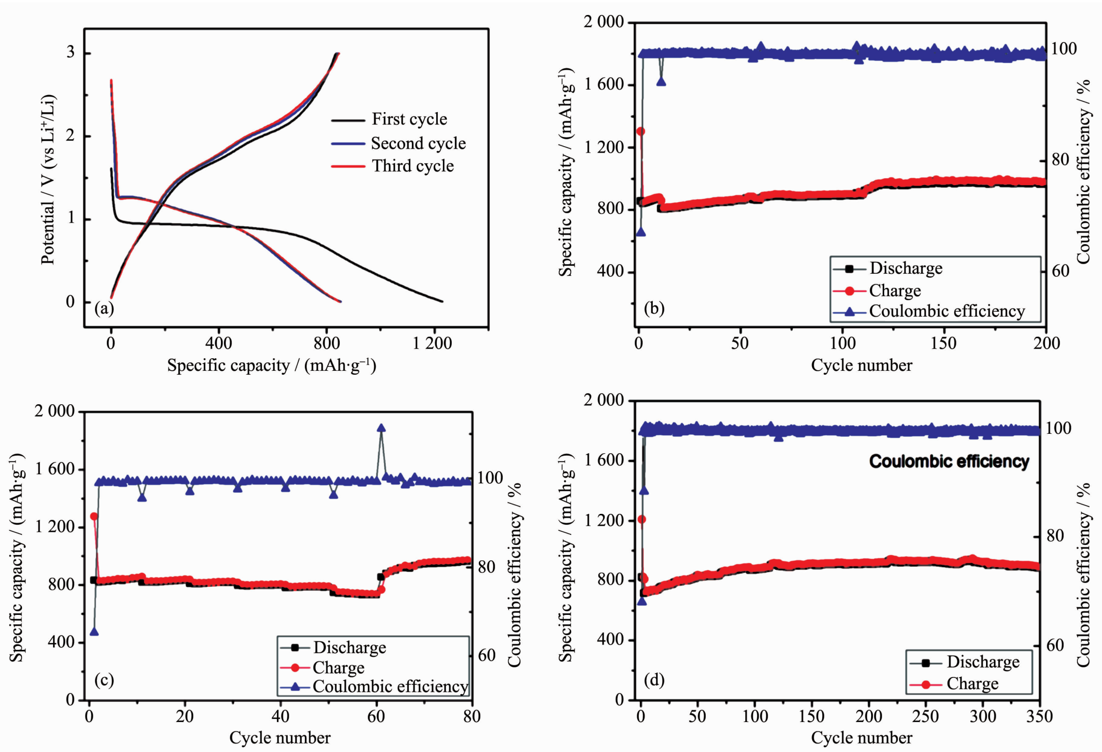

Fig.5 (a) Typical charge-discharge curves for selected cycles of $ZnCo_2O_4$ microspheres at 0.2 A·g^{-1}; Cycling performances at different current densities: (b) 0.5 A·g^{-1}, (d) 0.8 A·g^{-1}; (c) Rate performance of the $ZnCo_2O_4$ microspheres

68% for the first cycle up to 90% for the second cycle, and then maintains at about 98% for the subsequent cycles.

Fig.5c shows the rate performance at a current density ranging from 0.2 to 2.0 A·g^{-1}. The $ZnCo_2O_4$ microspheres deliver the reversible capacity of 846, 823, 810, 800, 786, and 736 mAh·g^{-1} at the current density of 0.2, 0.4, 0.6, 0.8, 1.0 and 2.0 A·g^{-1}, respectively. As the current density is returned back to 0.2 A·g^{-1}, the specific capacity of 980 mAh·g^{-1} is retained, indicating fine rate performance.

At a higher current density of 0.8 A·g^{-1}, the $ZnCo_2O_4$ microspheres shows a reversible capacity of 882 mAh·g^{-1} after 350 cycles, as shown in Fig.5d. The slight capacity increase was common for several mental oxides anode materials, which could be explained by the activation process of inner metal oxides electrode during cycling and the reversible growth of polymeric gel-like films caused by kinetically activated electrolyte degradation[3-4,6,14]. The columbic efficiency is able to reach above 98% after two cycles, which was important for practical application.

Electrochemical impedance spectroscopy (EIS) of the $ZnCo_2O_4$ microspheres electrode was measured before cycling and after 10 cycles. Fig.6 shows the Nyquist plots. A semicircle in the high-frequency range was assigned to the charge transfer impedance in the electrode/electrolyte interface, and an inclined line in the low-frequency range was corresponding to the Li-ion diffusion process[5]. Remarkably, the surface layer resistance was increased significantly after 10 cycles, which was mainly caused by the formation of SEI film[16]. Fig.7 displays SEM image of the cycled $ZnCo_2O_4$ microspheres electrode. It was clearly to find that the diameter of these microspheres increased up to over 4 μm, but still maintained their initial structure integrity, which was significant to improve the cycling stability of the electrode.

The improved electrochemical performance such as high specific capacity, good cycling stability and rate capability of the as-synthesized clew-like $ZnCo_2O_4$ microspheres should be ascribed to the multi-advantageous structure of the $ZnCo_2O_4$. First, primary

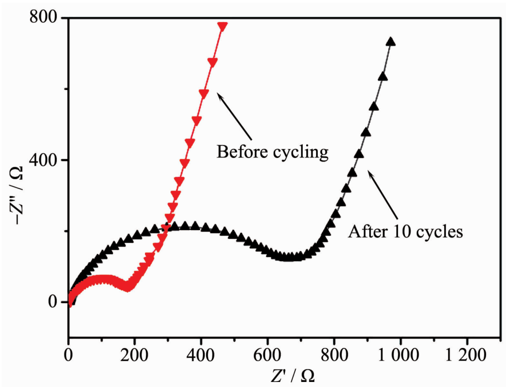

Fig.6　EIS of $ZnCo_2O_4$ microspheres electrode before and after cycling

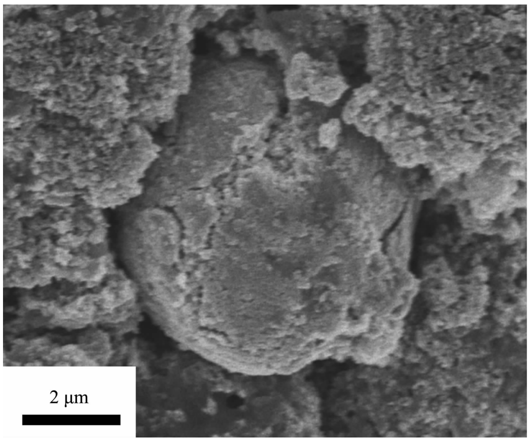

Fig.7　SEM image of $ZnCo_2O_4$ microspheres electrode after 200 cycles

$ZnCo_2O_4$ nanoparticles could effectively release the strain induced by volume changes, thus preventing the active materials from cracking. Second, the clew-like hierarchical microspheres have stable mechanical skeleton, which prevent the active materials pulverization during lithium-ion insertion/extraction process. Whats more, a large amount of nano-sized pores throughout the microspheres would not only offer diffusion channels for fast electric and ionic diffusion, but also provide void space to buffer volume variation.

3　Conclusions

In summary, hierarchical clew-like $ZnCo_2O_4$ microspheres composed of interconnected uniform nanoparticles was synthesized through a simple method, which is easily to scale up. As an anode for rechargeable lithium-ion batteries, the obtained clew-like $ZnCo_2O_4$ microspheres deliver reversible capacity of 965 mAh·g^{-1} at a current density of 0.5 A·g^{-1} after 200 cycles. At a higher current density of 0.8 A·g^{-1}, the $ZnCo_2O_4$ microspheres still deliver a reversible capacity of 882 mAh·g^{-1} even over 350 cycles. The superior electrochemical performance such as high specific capacity, good cycling stability and rate capability is attributed to the unique architecture. This study paves a way to explore the promising anode material for next-generation rechargeable lithium-ion batteries.

Supporting information is available at http://www.wjhxxb.cn

References:

[1] Park J, Moon W G, Kim G P, et al. *Electrochim. Acta*, **2013**, **105**:110-114

[2] Zhang X X, Xie Q S, Yue G H, et al. *Electrochim. Acta*, **2013**,**111**:746-75

[3] Sharma Y, Sharma N, Subba Rao G V, et al. *Adv. Funct. Mater.*, **2007**,**17**(15):2855-2861

[4] Liu B, Zhang J, Wang X F, et al. *Nano Lett.*, **2012**,**12**(6): 3005-3011

[5] Liu H W, Wang J. *Electrochim. Acta*, **2013**,**92**:371-375

[6] Luo W, Hu X L, Sun Y M, et al. *J. Mater. Chem.*, **2012**,**22** (18):8916-8921

[7] Qiu Y C, Xu G L, Yan K Y, et al. *J. Mater. Chem.*, **2011**,**21** (17):6346-6353

[8] Du N, Xu Y F, Zhang H, et al. *Inorg. Chem.*, **2011**,**50**(8): 3320-3324

[9] Chou S L, Wang J Z, Liu H K, et al. *J. Phys. Chem. C*, **2011**,**115**(32):16220-16227

[10]Zhong K F, Zhang B, Luo S H, et al. *J. Power Sources*, **2011**,**196**(16):6802-6808

[11]Yang J, Zhou X Y, Zou Y L, et al. *Electrochim. Acta*, **2011**, **56**(24):8576-8581

[12]Bai J, Li X G, Liu G Z, et al. *Adv. Funct. Mater.*, **2014**,**24** (20):3012-3020

[13]Li J F, Wang J Z, Wexler D, et al. *J. Mater. Chem. A*, **2013**, **1**(48):15292-15299

[14]Liu B, Liu B Y, Wang Q F, et al. *ACS Appl. Mater. Inter.*, **2013**,**5**(20):10011-10017

[15]Reddy M V, Kenrick K Y H, Wei T Y, et al. *J. Electrochem. Soc.*, **2011**,**158**(12):A1423-A1430

[16]Chen C H, Liu J, Amine K. *J. Power Sources*, **2001**,**96**(2): 321-328